Effect of Annealing Temperature of Ni-P/Si on its Lithiation and Delithiation Properties

Journal of The Electrochemical Society, 2020 **167** 040512

Effect of Annealing Temperature of Ni-P/Si on its Lithiation and Delithiation Properties

Yasuhiro Domi,[1,2] Hiroyuki Usui,[1,2] Ayumu Ueno,[1,2] Yoshiko Shindo,[2,3] Hayato Mizuguchi,[1,2] Takuro Komura,[2,3] Toshiki Nokami,[1,2] Toshiyuki Itoh,[1,2] and Hiroki Sakaguchi[1,2,*,z]

[1]*Department of Chemistry and Biotechnology, Graduate School of Engineering, Tottori University, Koyama–cho, Tottori 680–8552, Japan*
[2]*Center for Research on Green Sustainable Chemistry, Tottori University, Koyama–cho, Tottori 680–8552, Japan*
[3]*Course of Chemistry and Biotechnology, Department of Engineering, Graduate School of Sustainability Science, Tottori University, Koyama–cho, Tottori 680–8552, Japan*

Annealed Ni–P–coated Si (Ni–P/Si) anodes for lithium-ion batteries have shown a superior cycle life with discharge capacity of 1000 mA h g^{-1} over 1100 cycles in some ionic-liquid electrolytes. However, the annealing temperature has yet to be optimized for Ni–P/Si electrodes. We investigated the electrochemical performance of Ni–P/Si electrode annealed at various temperatures in this study. The Ni–P/Si electrodes annealed at 800 ± 20 °C exhibited a superior cycle life with a reversible capacity of 1000 mA h g^{-1} over 1000 cycles, whereas the capacity of the electrodes annealed at temperatures of 750 °C and 850 °C faded at approximately 500 cycles. At 800 °C, a newly formed $NiSi_2$ phase was theorized to significantly contribute to improving adhesion between the Ni–P coating layer and the Si particles. The Ni–P coating particles tended to aggregate at 850 °C, leading to a reduction in the coating effect, that is, a decline in their reactivity with Li^+, acceleration of electrode disintegration, and a reduction in electrical conductivity. On the other hand, Ni–P/Si electrodes annealed at 850 °C exhibited a superior rate performance. The amount of available $NiSi_2$ which ultimately contributed to higher reactivity with Li should increase.
 [DOI: 10.1149/1945-7111/ab743f]

Manuscript submitted November 20, 2019; revised manuscript received January 27, 2020. Published February 17, 2020.

Supplementary material for this article is available online

The advent of both electric and hybrid electric vehicles plays a key role toward the goal of increasing sustainability in society. To this end, there is high demand for lithium-ion batteries (LIBs) with a high energy density, longer cycle life, and higher safety margins.[1–3] Even though silicon (Si) has attracted much attention as an anode active material for next-generation LIBs due to its high theoretical capacity of 3580 mA h g^{-1},[4,5] it is known to expand and contract during lithiation (charge) and delithiation (discharge) reactions, respectively. The phase transition from Si to crystalline $Li_{15}Si_4$ (c-$Li_{15}Si_4$) occurs at a volume expansion rate of 280%, which increases stress and strain factors within the active material.[6] This strain accumulates over the course of repeated lithiation-delithiation cycles, thus causing pulverization or cracking of the Si particles. This eventually leads to disintegration of the anode and a marked reduction in its reversible capacity. Additionally, a low Li^+ diffusion coefficient, high electrical resistivity, hardness, and friability make Si a poor choice as an active material in next-generation LIBs.

Many approaches were proposed to address these issues, including coating Si with carbon to improve its electrical conductivity,[7] applying a film-forming additive or an ionic-liquid electrolyte to generate a stable surface film,[8–10] synthesizing nanostructured materials which will accommodate the inevitable volume expansion,[11–13] as well as "doping" the Si with impurities in an effort to reduce its electrical resistivity and to change physical properties related to phase transition, crystallinity, and morphology.[14–17] Integrating composite electrodes made of elemental Si and other materials which are capable of complementing and countering these disadvantages have been proven useful in the past.[18–21] These composite materials have been shown to possess four main properties: (1) mechanical properties which alleviate the stress generated through successive Si-lithiation and delithiation cycles, (2) moderate reactivity with Li^+ that does not to prevent Li^+ diffusion into Si, (3) high electrical conductivity which complements the poor conductivity of elemental Si, and (4) high thermodynamic stability that does not decompose under repeated lithiation-delithiation cycles.

The Ni–P–coated Si (Ni–P/Si) electrode is one of the more favorable composite electrodes that have been proposed due to its impressive electrochemical performance.[22–25] In a propylene carbonate (PC)-based organic electrolyte, the electrode has been shown to possess an initial reversible capacity of ca. 2600 mA h g^{-1} at the 20th cycle and maintains a discharge capacity of 780 mA h g^{-1} even after the 1000th cycle. Ni–P/Si electrodes are typically prepared via Electroless Deposition (ELD)[26,27] and subsequent Gas-Deposition (GD).[28] The Ni–P coating layers can play important roles in alleviating the stress induced by a change in the volume of Si and in increasing the electrical conductivity of the active material. In addition, since the Ni–P layer consists of both Ni and Ni_3P, Ni_3P acts as a Li^+ diffusion pathway due to its moderate reactivity with Li^+.[29] Annealed Ni–P/(etched Si) electrodes have a longer cycle life with discharge capacities of 1000 mA h g^{-1} over 1100 cycles in some ionic-liquid electrolytes.[24,25] However, the annealing temperature has yet to be optimized for Ni–P/Si electrodes. In the present study, the effect of annealing temperature of the Ni–P/Si particle was investigated in relation to its lithiation and delithiation properties.

Experimental

Synthesis and characterization of various Ni–P/Si powders.—Si particle (diameter: ca. 2 μm) was coated with Ni–P particles by the ELD method.[22,23] The Ni–P/Si powders were annealed at various temperatures (750, 780, 800, 820, and 850 °C) in an inert gas atmosphere. In the initial state (before annealing of Ni–P composite), the ratio the ratio of Ni-P to Si was 4.68 to 95.32 wt% (Ni:P = 4.54:0.14 wt%) which was estimated by inductively coupled plasma-atomic emission spectroscopy. The Ni–P/Si powders were synthesized by Hitachi Metals Neomaterial, Ltd.

The crystal structures of the prepared Ni–P/Si powders were determined using X-ray diffraction (XRD, Ultima IV, Rigaku) with Cu-Kα radiation. The voltage and current were determined to be 40 kV and 40 mA, respectively. Crystal phases were identified based on standard data obtained from the Inorganic Crystal Structure Database (ICSD), whereas Backscattered Electron (BSE) images

*Electrochemical Society Member.
[z]E-mail: sakaguch@chem.tottori–u.ac.jp

were acquired using a Field-Emission Scanning Electron Microscope (FE-SEM, JSM-7800F, JEOL Ltd.) equipped with an Energy-Dispersive X-ray Spectroscope (EDS). The beam acceleration voltage and working distance were set at 5 kV and 10 mm, respectively, and the surface of the Ni–P/Si particles was coated with gold to prevent charge-up. Morphology and selected area electron diffraction (SAED) patterns for the Ni–P/Si particles were also acquired using a Transmission Electron Microscope (TEM, JEM-ARM200F, JEOL Ltd.).

Electrode preparation.—A Ni–P/Si thick-film electrode was prepared by GD using He as a carrier gas. Other detailed GD conditions were previously reported.[14] The weight of the deposited active materials on the Cu current collector (thickness: 20 μm) was 30 ± 2 μg. A 2032-type coin cell consisting of the Ni–P/Si electrode as a working electrode, a glass fiber filter (Whatman GF/A) as a separator, and a Li metal foil (Rare Metallic Co., Ltd., 99.9%, thickness: 1 mm) as a counter electrode was assembled. The ionic-liquid electrode used in this study was 1 mol dm^{-3} (M) lithium bis (fluorosulfonyl)amide (LiFSA) dissolved in *N*-methyl-*N*-propylpyrrolidinium bis(fluorosulfonyl)amide (Py13-FSA). Cell assembly and electrolyte preparation were performed in an Ar-filled glovebox (Miwa MFG, DBO-2.5LNKP-TS) in which the dew point was less than −100 °C and O_2 concentration was kept below 1 ppm.

Electrochemical measurement.—Galvanostatic charge-discharge testing was performed using an electrochemical measurement system (HJ-1001SM8 or HJ-1001SD8, Hokuto Denko Co., Ltd.) in the potential range between 0.005 and 2.000 V vs Li^+/Li at 303 K. The electrode's cycle life was investigated under a charge capacity limit of 1000 mA h g^{-1} at a current density of 0.36 A g^{-1} (0.1 *C*) during the first cycle and 1.44 A g^{-1} (0.4 *C*) during the subsequent cycles. Rate performance was also estimated between 1 and 50 *C* with a charge capacity limit of 1000 mA h g^{-1} after pre-cycling. The pre-cycling was performed following procedures to form stable film between the electrode and electrolyte interphase; the Ni–P/Si electrode was charged from an open circuit voltage (OCV) to 0.500 V vs Li^+/Li at a *C*-rate of 0.1 *C*, maintained at 0.500 V vs Li^+/Li for 12 h, and then discharged from 0.500 to 2.000 V vs Li^+/Li at 0.1 *C*.

Results and Discussion

Characterization of Ni–P/Si particles annealed at various temperature.—Figure 1 shows XRD patterns acquired for Ni–P/Si powders annealed at various temperatures. When annealed at 750 °C, peak intensities of Ni (111) and Ni (200) were shown to increase and there was the appearance of a peak which was subsequently assigned to NiSi (112). These results indicated that the crystallinity of Ni increased, and that some of the Ni atoms in the coating layer had diffused into the Si particles to form a NiSi phase. At 780 °C, the peak intensities of the Ni phases showed a marked decline. Whereas a definitive XRD peak for $NiSi_2$ (220) was not confirmed at around 47.5° due to an overlap with the peak assigned to Si (220), it was presumed that the $NiSi_2$ phase was formed considering the reduction observed in the size of the peak assigned to the NiSi phase. In addition, literature reports confirm that the $NiSi_2$ phase typically forms after annealing at 800 °C.[30]

To verify the formation of the $NiSi_2$ phase, we measured a SAED pattern for Ni–P/Si particles annealed at 800 °C (Fig. S1 is available online at stacks.iop.org/JES/167/040512/mmedia), and the d-spacings derived from this analysis were summarized in Table I. The results revealed that the Ni–P coating layer consisted of NiSi, $NiSi_2$, Ni_3P, and Ni. Since the Ni_3P and Ni phases had been detected without annealing and the NiSi phase had been confirmed at 750 °C (see Fig. 1), the $NiSi_2$ phase must have been formed at 800 °C. Thus, nickel silicides (NiSi and $NiSi_2$) should have been formed at the interface between the Ni–P coating layer and the Si particles. In Fig. 1, it was clear that the peaks assigned to the Ni and NiSi phases

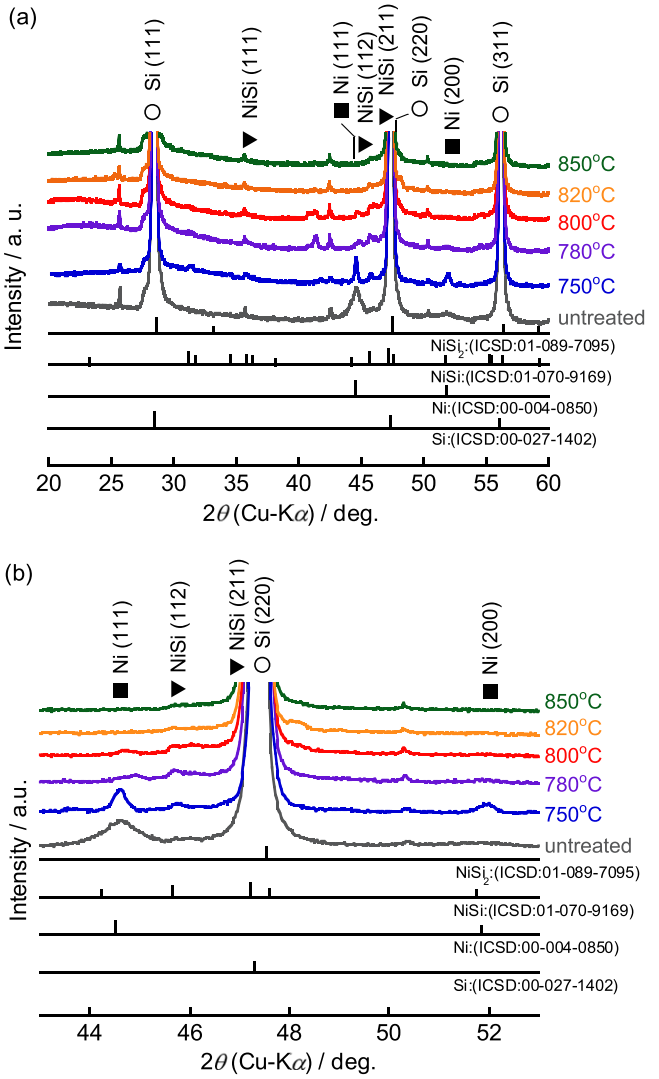

Figure 1. (a) Complete XRD patterns of Ni–P/Si powders annealed at various temperatures and (b) its enlarged view.

disappeared at 850 °C, which was indicative of a complete reaction between the Ni atoms and the Si particles as well as transformation to the $NiSi_2$ phase.

Figure 2 displays the BSE images acquired for Ni–P/Si powders annealed at various temperatures and their corresponding EDS maps. Since BSE images typically reflected the electron density of the sample under investigation, the light spots seen in Fig. 2 were believed to correspond to Ni–P. The images showed that Ni–P did not coat the Si surface in layers but rather in patches, regardless of the annealing temperature being used. Table II summarizes the Ni–P particle size on Si at various annealing temperatures. The size of Ni–P particles annealed at 750 °C was almost the same as that seen in particles annealed at 800 °C. Conversely, the size of Ni–P particles annealed at 850 °C was about 1.6 times larger than those annealed at other temperatures, which indicated that particle aggregation occurred at elevated temperatures.

Effect of annealing temperature of Ni–P/Si particle on its cycling performance.—We firstly investigated the effect of Ni–P/Si particle size and electrolyte on its electrochemical performance for LIBs. Figure S2 shows the typical electrochemical performances of Ni–P/Si electrodes with diameters of 2 and 10 μm in 1 M LiFSA/Py13-FSA. The 2 μm electrode exhibited better cycle life cycle life and rate performance. The superior cycle life could be attributed to

Table I. Summary of *d*-spacings and crystal phase data derived from selected area electron diffraction analysis of Ni–P/Si particle annealed at 800 °C. The table includes ICSD standard *d*-spacing values for Si (No. 00–027–1402) Ni (No. 00–004–0850), NiSi (No. 01–070–-9170), $NiSi_2$ (No. 01–089–7095), and Ni_3P (No. 01–074–3245).

SAED	ICSD	
d-spacing/nm	*d*-spacing/nm	Crystal phase (*h k l*)
0.3184	0.3164	Ni_3P (2 2 0)
0.2780	0.2703	$NiSi_2$ (2 0 0)
0.1954	0.1945	Ni_3P (1 4 1)
0.1673	0.1662	NiSi (0 2 0)
0.1178	0.1179	NiSi (4 0 2)
0.1061	0.1062	Ni (3 1 1)
0.0918	0.0918	Si (5 3 1)

the multifaceted impact of the "Ni–P coating effect" which included making improvements in the electrode's reactivity with Li^+, suppressing electrode disintegration, and increasing electrical conductivity. All of this was thought to be the result of the higher numbers of interphase points between the Ni–P coating layer and the Si particles caused by a reduction in Si particle size. In addition to the impact of the Ni–P coating effect, the Si utilization rate was also expected to increase due to the shortening of the Li^+ diffusion path; thus, the Ni–P/Si electrodes which consisted of smaller particles were theorized to exhibit exquisite rate capability. Therefore, Ni–P/Si electrodes with a diameter of 2 μm became the focal point of our study hereafter, unless otherwise stated. Since not all ionic-liquid electrolytes were shown to improve the electrochemical performance of Ni–P/Si anode,[30] we optimized ionic-liquid electrolyte (Figs. S3 and S4). As a result, superior cycle life and rate performance were obtained in 1 M LiFSA/Py13-FSA. We have also reported that Si-based electrodes exhibit better cycling performance in this

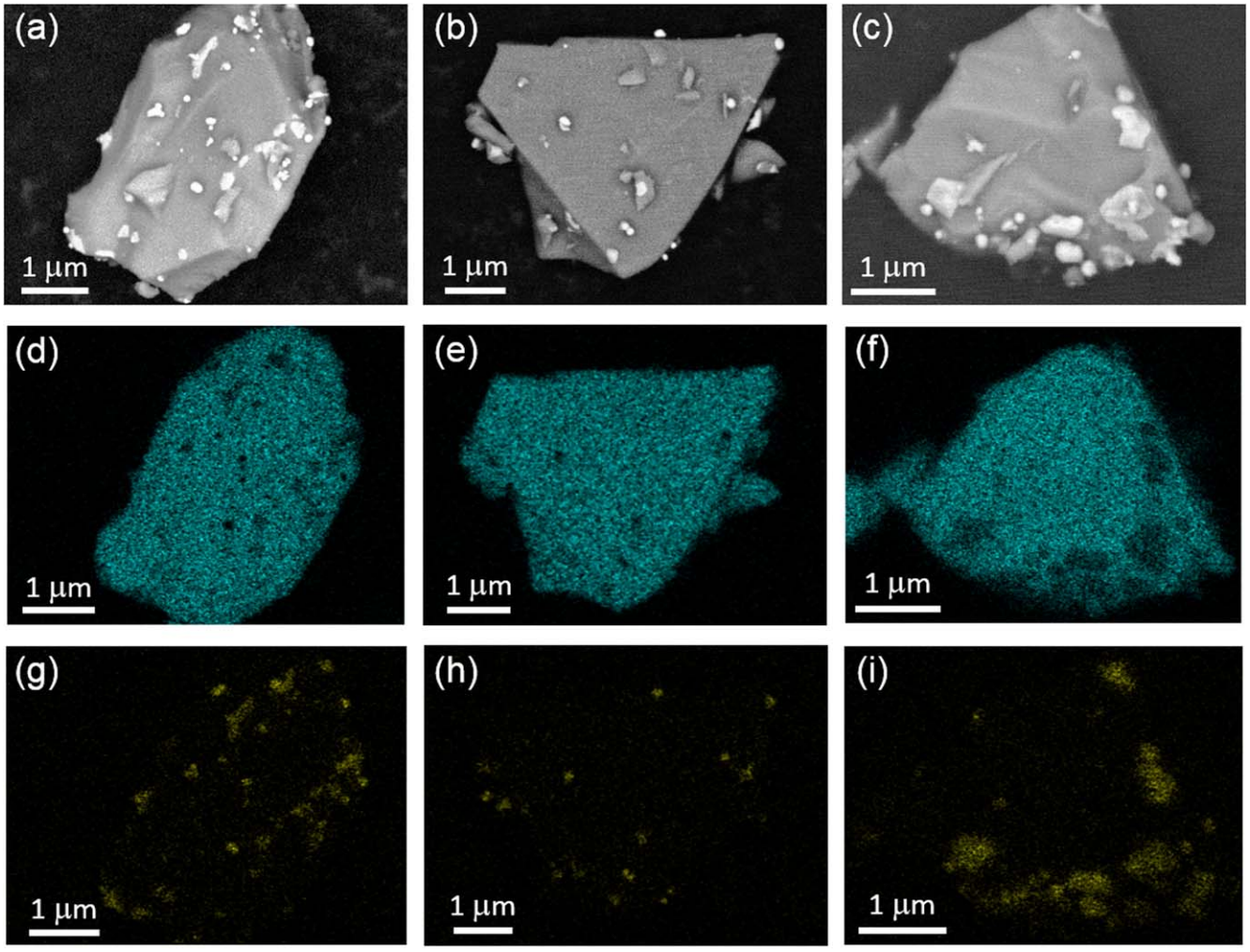

Figure 2. (a)–(c) BSE images and (d)–(i) the corresponding EDS maps for the Ni–P/Si powders. The powders were annealed at (left) 750, (middle) 800, and (right) 850 °C. Parts (d)–(f) and (g)–(i) represent the elements Si and Ni, respectively.

Table II. Ni–P particle size on Si annealed at various temperatures.

Temperature/°C	Particle size/μm
750	0.15 ± 0.04
800	0.13 ± 0.03
850	0.22 ± 0.10

electrolyte.[17,31,32]

Figure 3 shows charge and discharge curves of Ni–P/Si electrodes annealed at various temperatures with a charge capacity limit of 1000 mA h g^{-1} in 1 M LiFSA/Py13-FSA. In the first cycle, the electrodes exhibited a potential slope below 2 V vs Li^+/Li on charge curve. Additionally, the charge capacity reached 1000 mA h g^{-1}, whereas the discharge capacity didn't reach 1000 mA h g^{-1}. The results demonstrate that the reductive decomposition of the ionic-liquid electrolyte occurs below 2 V vs Li^+/Li and the electrodes

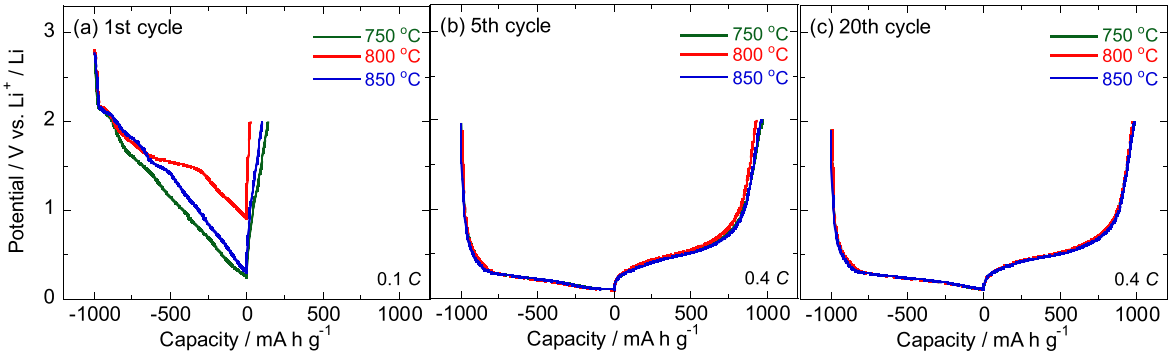

Figure 3. (a) first, (b) fifth, and (c) twentieth charge and discharge curves of Ni–P/Si electrodes annealed at various temperatures with a charge capacity limit of 1000 mA h g^{-1} in 1 M LiFSA/Py13-FSA.

didn't store the amount of Li^+ corresponding to 1000 mA h g^{-1}. We confirmed potential plateaus at around 0.2 and 0.4 V vs Li^+/Li on charge and discharge curves regardless of the annealing temperature, respectively (Figs. 3b and 3c).[33] The plateaus are attributed to the alloying and dealloying reactions of Si with Li.

The cycle life of Ni–P/Si electrodes annealed at various temperatures with a charge capacity limit of 1000 mA h g^{-1} in 1 M LiFSA/Py13-FSA is depicted in Fig. 4. A Ni–P/Si electrode that had been annealed at 780, 800 and 820 °C maintained a discharge capacity of 1000 mA h g^{-1} over 1000 cycles, whereas the capacity of Ni–P/Si electrodes that were annealed at 750 °C and 850 °C faded after approximately 500 cycles. When the discharge capacity faded, an electrode disintegration can occur. Based on Fig. 1 and Table I, the NiSi phase was formed at 750 °C, while both NiSi and $NiSi_2$ phases were formed at 800 °C. Given this, it could be theorized that the newly formed $NiSi_2$ phase at around 800 °C significantly contributed to improving overall adhesion between the Ni–P coating layer and the Si particles (inset in Fig. 4). Noteworthy also was the fact that Ni–P coating particles tended to aggregate with each other at 850 °C (Fig. 2 and Table II), which theoretically, led to a reduction in the aforementioned "coating effect." Therefore, the results show that Ni–P/Si electrodes annealed at 800 °C exhibited the longest cycle life of the lot and suppressed its disintegration.

Rate performance of Ni–P/Si electrodes annealed at various temperature.—Figure 5 shows the rate capability of Ni–P/Si electrodes annealed at various temperatures with a charge capacity limit of 1000 mA h g^{-1} in 1 M LiFSA/Py13-FSA. The rate performance of Ni–P/Si electrodes annealed at 800 °C was almost the same as that seen in electrodes annealed at 750 °C. By contrast, the electrodes annealed at 850 °C exhibited higher reversible capacity at higher *C*-rates (20 and 50 *C*) when compared to the other two electrodes. This order of rate capability cannot be accounted for through simple aggregation of Ni–P coating particles. The discharge capacity of all three electrodes recovered after the 31st cycle when the *C*-rate was lowered to 0.1 *C*. This indicated that no electrode disintegration occurred.

The number of available Ni and NiSi was shown to decrease when the annealing temperature was increased, whereas the amount of $NiSi_2$ increased as described above. The amount of Ni_3P would not be changed depending on annealing temperature. The electronic resistivity of NiSi, $NiSi_2$, and Ni_3P included in the coating layer was 14, 34, and 120 $\mu\Omega$ cm, respectively, whereas the resistivity of $NiSi_2$ was not smaller than that observed for the others.[34,35] That is, the difference of rate performance between annealing temperature cannot explain electronic resistivity. So, it was assumed that reactivity of $NiSi_2$ with Li^+ was higher than that of NiSi; hence, the Ni–P/Si electrodes annealed at 850 °C exhibited a superior rate performance. We have previously reported that $NiSi_2$ electrode exhibited high reactivity with Li in Py13-FSA-based ionic-liquid electrolyte.[36] To confirm this assumption, we investigated cycling performance of each nickel silicide electrode (Fig. 6). The $NiSi_2$-

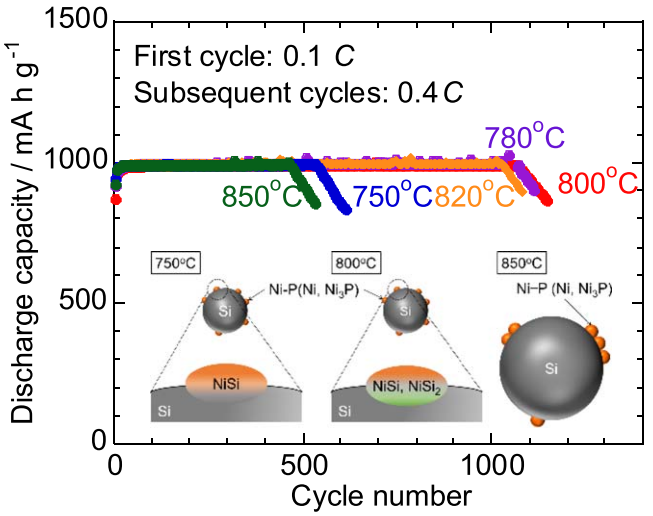

Figure 4. Cycle life of Ni–P/Si electrodes annealed at various temperatures with a charge capacity limit of 1000 mA h g^{-1} in 1 M LiFSA/Py13-FSA.

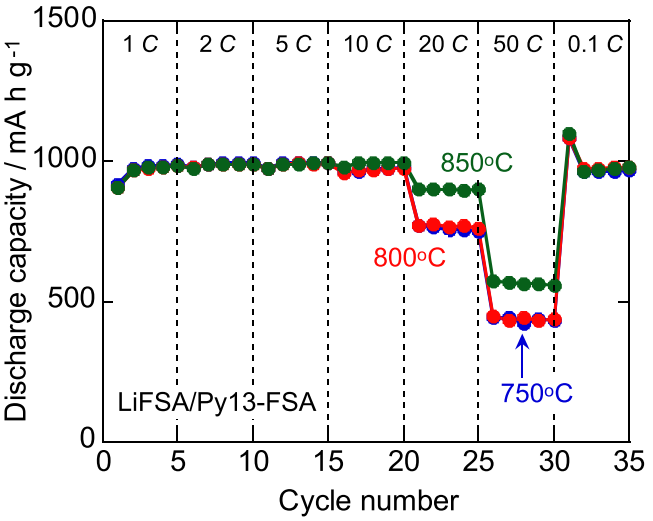

Figure 5. Rate capability of Ni–P/Si electrodes annealed at various temperatures with a charge capacity limit of 1000 mA h g^{-1} in 1 M LiFSA/Py13-FSA.

and NiSi-alone electrodes exhibited an initial discharge capacity of about 820 and 250 mA h g^{-1}, respectively. The $NiSi_2$-alone electrode also maintained higher reversible capacity even after the 100th cycle: the capacity retention is 86% and 56% for $NiSi_2$ and NiSi electrodes, respectively. Consequently, it is demonstrated that the

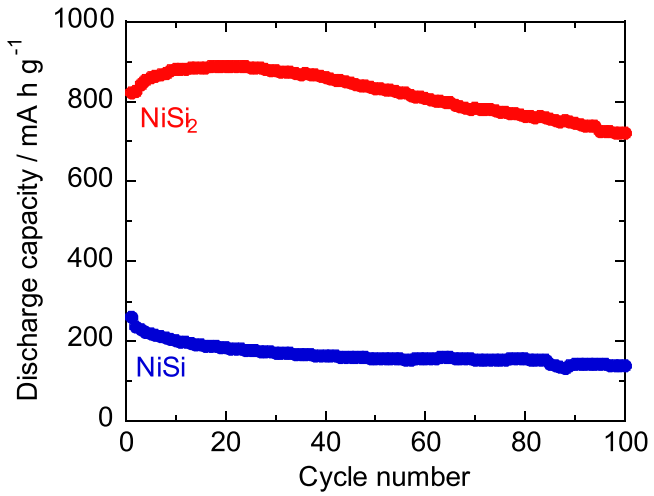

Figure 6. Cycling performance of $NiSi_2$- and NiSi-alone electrodes in 1 M LiFSA/Py13-FSA at current rate of 50 mA g^{-1} without a charge capacity limit.

above assumption is valid and the best rate performance at 850 °C is attributed to high reactivity of $NiSi_2$ with Li. It is noted that the capacity which was assumed by $NiSi_x$ is limited because the amount of $NiSi_x$ is less than 10 wt%. If all elemental Ni transforms nickel silicide (the ratio of NiSi to $NiSi_2$ is 1:1) after annealing, we calculated each ratio by weight as follows; Si: NiSi: $NiSi_2$: Ni_3P = 91.21: 3.37: 4.46: 0.96 wt%.

Conclusions

We investigated the effect of annealing temperature of Ni–P/Si on its electrochemical performance for LIBs. The electrodes annealed at 800 ± 20 °C maintained a capacity of 1000 mA h g^{-1} over the course of 1000 cycles, whereas the discharge capacity of Ni–P/Si electrodes annealed at 750 °C and 850 °C faded after approximately 500 cycles. It was theorized that the newly formed $NiSi_2$ phase at 800 °C significantly contributed to improving adhesion between the Ni–P coating layer and the Si particles. Ni–P coating particles aggregated with each other at 850 °C, which led to a notable reduction in the coating effects. By contrast, the Ni–P/Si electrodes annealed at 850 °C exhibited a superior rate capability. $NiSi_2$ mostly formed at 850 °C and its reactivity with Li was higher compared with NiSi.

Acknowledgments

This work was partially supported by the Japan Society for the Promotion of Science (JSPS) KAKENHI (grant numbers 19K05649, 19H02817, and 17H03128) and the MEXT Program for Development of Environmental Technology using Nanotechnology. The authors gratefully acknowledge Ryoji Inoue (Hitachi Metals Neomaterial Ltd.) and Ken Asada (Hitachi Metals Neomaterial Ltd.) for their assistance with the synthesis of variously treated Ni–P powders.

References

1. M. S. Whittingham, *Chem. Rev.*, **104**, 4271 (2004).
2. M. Armand and J.-M. Tarascon, *Nature*, **451**, 652 (2008).
3. J. B. Goodenough and Y. Kim, *Chem. Mater.*, **22**, 587 (2010).
4. S.-C. Lai, *J. Electrochem. Soc.*, **123**, 1196 (1976).
5. M. N. Obrovac and L. J. Krause, *J. Electrochem. Soc.*, **154**, A103 (2007).
6. X. H. Liu, L. Zhong, S. Huang, S. X. Mao, T. Zhu, and J. Y. Huang, *ACS Nano*, **6**, 1522 (2012).
7. X. Zhou, Y.-X. Yin, A.-M. Cao, L.-J. Wan, and Y.-G. Guo, *ACS Appl. Mater. Interfaces*, **4**, 2824 (2012).
8. Y. Domi, H. Usui, M. Shimizu, K. Miwa, and H. Sakaguchi, *Int. J. Electrochem. Sci.*, **10**, 9678 (2015).
9. M. Haruta, R. Hioki, T. Moriyasu, A. Tomita, T. Takenaka, T. Doi, and M. Inaba, *Electrochim. Acta*, **267**, 94 (2018).
10. D. M. Piper et al., *Nat. Commun.*, **6**, 6230 (2015).
11. M. T. McDowell, I. Ryu, S. W. Lee, C. Wang, W. D. Nix, and Y. Cui, *Adv. Mater.*, **24**, 6034 (2012).
12. X. Zhou, L.-J. Wan, and Y.-G. Guo, *Small*, **9**, 2684 (2013).
13. B. Liu, X. Wang, H. Chen, Z. Wang, D. Chen, Y.-B. Cheng, C. Zhou, and G. Shen, *Sci. Rep.*, **3**, 1622 (2013).
14. Y. Domi, H. Usui, M. Shimizu, Y. Kakimoto, and H. Sakaguchi, *ACS Appl. Mater. Interfaces*, **8**, 7125 (2016).
15. B. R. Long, M. K. Y. Chen, J. P. Greeley, and A. A. Gewirth, *J. Phys. Chem. C*, **115**, 18916 (2011).
16. R. Yi, J. Zai, F. Dai, M. L. Gordin, and D. Wang, *Electrochem. Commun.*, **36**, 29 (2013).
17. S. Yodoya, Y. Domi, H. Usui, and H. Sakaguchi, *ChemistrySelect*, **4**, 1375 (2019).
18. H. Usui, K. Nouno, Y. Takemoto, K. Nakada, A. Ishii, and H. Sakaguchi, *J. Power Sources*, **268**, 848 (2014).
19. Y. Domi, H. Usui, Y. Takemoto, K. Yamaguchi, and H. Sakaguchi, *J. Phys. Chem. C*, **120**, 16333 (2016).
20. H. Usui, Y. Kashiwa, T. Iida, and H. Sakaguchi, *J. Power Sources*, **195**, 3649 (2010).
21. H. Usui, N. Uchida, and H. Sakaguchi, *J. Power Sources*, **196**, 10244 (2011).
22. H. Usui, M. Shibata, K. Nakai, and H. Sakaguchi, *J. Power Sources*, **196**, 2143 (2011).
23. H. Usui, N. Uchida, and H. Sakaguchi, *Electrochemistry*, **80**, 737 (2012).
24. Y. Domi, H. Usui, M. Narita, Y. Fujita, K. Yamaguchi, and H. Sakaguchi, *J. Electrochem. Soc.*, **164**, A3208 (2017).
25. K. Yamaguchi, Y. Domi, H. Usui, A. Ueno, T. Komura, T. Nokami, T. Itoh, and H. Sakaguchi, *Chem. Lett.*, **47**, 1416 (2018).
26. T. Cetinkaya, M. Uysal, M. O. Guler, H. Akbulut, and A. Alp, *Power Technol.*, **253**, 63 (2014).
27. G. Talla, R. K. Guduru, B. Q. Li, and P. S. Mohanty, *Solid State Ionics*, **269**, 8 (2015).
28. H. Sakaguchi, T. Toda, Y. Nagao, and T. Esaka, *Electrochem. Solid-State Lett.*, **10**, J146 (2007).
29. J. Y. Xiang, J. P. Tu, X. L. Wang, X. H. Huang, Y. F. Yuan, X. H. Xia, and Z. Y. Zeng, *J. Power Sources*, **185**, 519 (2008).
30. C. M. Liu, W. L. Liu, S. H. Hsieh, T. K. Tsai, and W. J. Chen, *Appl. Surf. Sci.*, **243**, 259 (2005).
31. Y. Domi, H. Usui, K. Yamaguchi, S. Yodoya, and H. Sakaguchi, *ACS Appl. Mater. Interfaces*, **11**, 2950 (2019).
32. Y. Domi, H. Usui, K. Sugimoto, and H. Sakaguchi, *Energy Technology*, **7**, 1800946 (2019).
33. K. Yamaguchi, Y. Domi, H. Usui, and H. Sakaguchi, *ChemElectroChem*, **4**, 3257 (2017).
34. E. G. Colgan, M. Mäenpaää, M. Finetti, and M.-A. Nicolet, *J. Electron. Mater.*, **12**, 413 (1983).
35. I. Koiwa, M. Usuda, and T. Osaka, *J. Electrochem. Soc.*, **135**, 1222 (1988).
36. Y. Domi, H. Usui, R. Takaishi, and H. Sakaguchi, *ChemElectroChem*, **6**, 581 (2019).